Hindawi
Advances in Materials Science and Engineering
Volume 2022, Article ID 3469305, 18 pages
https://doi.org/10.1155/2022/3469305

Research Article

Study on the Microstructure of Vanadium-Modified Tungsten High-Speed Steel-Coded SAE-AISI T1 Steel

Hossam Halfa,[1] **Asiful H. Seikh**,[2] **Hany S. Abdo**,[2,3] **Ibrahim A. Alnaser**,[2,4] **Mahmoud S. Soliman**,[4] **and Sameh M. Ragab**[2]

[1]*Steel Technology Department, Central Metallurgical R&D Institute (CMRDI), Helwan, Egypt*
[2]*Centre of Excellence for Research in Engineering Materials, Deanship of Scientific Research, King Saud University, PO Box 800, Riyadh 11421, Saudi Arabia*
[3]*Mechanical Design and Materials Department, Faculty of Energy Engineering, Aswan University, Aswan 81521, Egypt*
[4]*Mechanical Engineering Department, College of Engineering, King Saud University, PO Box 800, Al-Riyadh 11421, Saudi Arabia*

Correspondence should be addressed to Hossam Halfa; dr.hossam@cmrdi.sci.eg

Received 13 October 2022; Revised 14 November 2022; Accepted 17 December 2022; Published 30 December 2022

Academic Editor: Carlos Garcia Mateo

The essential goal of this research is to evaluate the modification process on phase transformation, matrix chemical composition, and precipitated carbide types for modified SAE-AISI T1 steel and their effects on the hardness values after optimum heat treatment conditions. This research adopts the alloying design strategy to enhance one of the most important tools steel coded SAE-AISI T1 (T12001). Therefore, two alloying enhancement processes took place through partial or total tungsten replacement. Investigated steel was modified first through the addition of vanadium and then through the addition of vanadium and carbon. Substitute 5 wt modified SAE-AISI T1 steel. % tungsten with 1 wt. % vanadium, in addition to carbon content, varied from 0 to 1 wt. %. Therefore, to fulfill the goals of this work, Thermo-Calc software was utilized to get the following: (i) thermodynamic equilibrium information, (ii) the expected microstructure, (iii) the constituent volume fraction, and (iv) carbide chemical composition. The chemical composition of the expected phases was confirmed by scanning electron microscopy (SEM) equipped with energy-dispersive X-ray (EDX). In addition, volume fractions of different constituents were estimated by using Thermo-Calc software and authenticated by the imaging analysis process. The experimental findings for the variations in the chemical composition of the matrix and eutectic carbides precipitated, e.g., MC and M_6C carbides, agree well with the calculated findings. Tungsten replacement by vanadium with and without extra carbon at traditional SAE-AISI T1 steel encourages MC carbide formation instead of M_6C, $M_{23}C_6$, and M_7C_3 carbides. MC carbide precipitated in vanadium with extra carbon-modified steel contains more carbon, chromium, and tungsten but less vanadium compared with vanadium-modified steel. Vanadium with extra carbon-modified steel precipitated more M_6C carbide and gamma-austenite. Hardness measurements emphasized that modified steel is a promising material for its use as a tooling material with low tungsten content and, in turn, produces cutting-tool materials with economical cost.

1. Introduction

Despite the competition in tooling materials, high-speed steel is utilized for forming material for multistage cutting and cold plastic forming tools. During the last two decades, the improvement trends of high-speed steel and tools made from them have depended mainly on the changes in production technology (e.g., powder technology methods [1–3], physical vaporization deposition (PVD) processes [4–6], and additive manufacturing methods [7]), as well as, alloying design strategy (e.g., introducing or substituting alloying elements into traditional high-speed steels [8–11]). High-speed steel deserves its name for the power of cutting various materials and rapid machining among other steel alloys. Furthermore, cutting properties are considered one of the most significant steel technological properties, which depend mainly on the resistance to heat tempering, impact, and wear. Impact strength is affected by the state of

a tempered matrix, grain size, classification of former austenite, volume fractions, spatial arrangement, and size distribution of primary carbide. The wear resistance of the investigated steel depends on the microstructure, the amount of primary carbide (MC and M_6C), and matrix hardness [12, 13]. High-speed steel microstructures should comprise high carbide volume fractions and high alloy matrices. The microstructure formed is recognized by homogeneous and fine distribution. The fine-mentioned microstructure is attributed to hard dissolving carbides during the austenitization process, which diminishes the growth of the matrix [14–16]. The microstructure of high-speed tool steel is controlled through the heat treatment procedure, as explained by the authors in [17–21].

This research aims to evaluate the effect of vanadium and vanadium with extra carbon modification for SAE-AISI T1 steel on the evolution temperature, amount, and chemical composition of precipitated carbide in addition to gamma-austenite and investigate the influence of the modification process on secondary hardening for enhanced SAE-AISI T1 steel after complete heat treatment, in addition to the obtained experimental results for modified steel compared with those for standard SAE-AISI T1 steel.

2. Materials and Methods

This work uses tungsten partially or fully substituted by a hard carbide-forming alloying element (vanadium) for investigating high-speed tool steels. In this approach, tungsten is substituted with vanadium: 5 wt. % of tungsten equivalent to 1 wt. % of vanadium. Furthermore, based on a designed carbon proportion content, the optimal influence of secondary hardening occurred when alloying elements and carbon contents matched the stoichiometric ratio of precipitated carbide [22].

In vanadium carbide (VC), the vanadium to carbon weight ratio is 1 : 0.235; however, the variation in higher vanadium content than the theoretical chemical proportion of VC forced the remaining amount of V to dissolve in the matrix after the formation of VC. We reduced carbon's matrix content because dissolving vanadium contributes to decreasing hardness of the investigated steel; however, raising carbon to a higher value than the chemical proportion of VC promoted precipitation of other carbides, and the remaining carbides dissolved in the matrix. The previous modification will positively affect hardness and wear properties of the investigated steel.

Raw materials were melted in a skull induction furnace to produce investigating steel ingots with 20kg capacity. Production conditions were documented elsewhere [23]. Throughout investigated steel production, the determined weight of ferroalloys (for example, ferrovanadium, ferromolybdenum, ferrotungsten, and ferrochromium) was added to carbon steel scrap. Carbon steel scrap was used as a base metal. After the additive material's complete melting, the molten steel's chemical composition was adjusted. Then, primary deoxidization was achieved utilizing strong deoxidizers such as ferromanganese, ferrosilicon, and aluminum.

Furthermore, ferrovanadium was added to primary deoxidization molten steel to improve vanadium absorptivity. The temperature and chemical composition of molten steel alloys were adjusted, while the final deoxidation process was conducted by adding 0.1% aluminum metal. Therefore, ferrovanadium was added to molten steel in the last stage of the melting process. Finally, at about 1500°C, molten steel alloys were poured out of the furnace into preheated cast iron chill molds at 700°C.

Thermodynamic equilibrium of vanadium modified and standard SAE-AISI T1 steel was estimated using the Thermo-Calc software. The multicomponent system Fe-C-Cr-W-V in Thermo-Calc was used to calculate the chemical composition of different phases present in the investigated steel. Many investigators performed a sublattice model, which stated all phases in the database [11, 24–26]. Phases other than those in the model have not been identified as suspected stable phases in the predictions exhibited here since they are not involved in standard high-speed steel alloys.

To obtain the correct microstructures of produced steel, it should be heat-treated as follows: packed, annealed at 870°C for 1 hour, gradually cooled in the furnace, and austenitized at different temperatures of 1000, 1100, 1150, 1200, and 1250°C for 5 minutes [27]. Steel specimens should be held at 450°C and then at 800°C for 5 minutes to equalize temperatures while heating the investigated steel. Then, austenitizing steel specimens were quenched by accelerating cooling (water cooling) followed by tempering three times at optimum conditions [27]. The optimum condition was determined by heating the quenched steel samples for 2 h in the temperature range from 400 to 650°C.

Blocks from the investigated steel of size 12 mm × 12 mm × 12 mm were cut after full heat treatment. Well-prepared specimens were used in hardness measurements, which were carried out using an Indemtec universal hardness testing machine with a 150 kg operating load. The average value was calculated from three test readings.

Well-prepared, polished, and etched specimens of nital (3%) are used to describe the microstructure and quantitatively discover the nature of different carbides encountered in the investigated steel. Accordingly, the microstructure and the nature of different carbides identified by scanning electron microscopy (SEM) are equipped with EDX. Three expected groups of carbides were observed in examining steels:

(i) MC is considered V-rich carbide

(ii) M_6C is considered W-rich carbide

(iii) $M_{23}C_6$ and M_7C_3 are considered Cr-rich carbides

Furthermore, as reported elsewhere, optical microscopy has been applied to separate each group of carbide using Groesbeck's reagent [28]. M_7C_3 and M_6C carbides were colored blue or yellow, while MC carbide was not etched and seemed pink in the martensite matrix. Moreover, M_7C_3 and M_6C carbides were monitored as one group when utilizing optical microscopy because they were always associated and had the same color. The laborer for every picture chose threshold levels interactively due to the nonreproducible

etching process from one specimen to another and seldom according to their surface's heterogeneity. Image processing is performed as follows:

(i) Carbides and the matrix are differentiated by simple thresholding.

(ii) MC carbide extracted encourages its average grey level.

(iii) Unknown pixels are $M_{23}C_6$, MC, and M_6C-M_7C_3 carbides.

(iv) Pixels are finally selected for one of the three carbide classes (MC, $M_{23}C_6$, and M_7C_3-M_6C) because of their grey level values.

For instance, the area inside and around carbide particles (M_7C_3, M_6C, and $M_{23}C_6$) and the matrix were digitized by pixels with grey level preferences equal to those of the MC-carbide level. Therefore, all M_7C_3, M_6C, and $M_{23}C_6$ carbides are classified as transition digital pixels from darker carbide to a bright matrix. Based on that, one specifies the basis of these pixels in the matrix.

An energy dispersive X-ray (EDX) point analyzer was qualitatively employed to identify the types of phases (carbide and matrix). Furthermore, the obtained data were used for matching with the published literature [29, 30]. Moreover, a wavelength dispersive X-ray (WDX) analyzer was qualitatively used to distinguish the carbide formula [31].

3. Results and Discussion

Due to a high amount of alloying additives in iron (C, W, V, Cr, etc.), high-speed tool steel (HSS) is considered a complex multicomponent system. Therefore, an enormous amount of time and work would be required to perform its experimental investigation. Therefore, considering these purposes for investigating the previous multicomponent system, many researchers have successfully utilized the CALPHAD method for phase equilibrium estimation [23, 32–37].

Thermo-Calc calculation was performed for investigating steel using chemical compositions determined by optical emission spectrometer (SPECTRO) measurements on the obtained steel alloys. Therefore, this research work divided investigated steels into two primary steel groups. The first group of steel consisted of constant carbon and differing vanadium contents. The second group of steel consisted of vanadium with extra carbon contents. Additionally, the investigated steel was compared with standard SAE-AISI T1 steel. Table 1 represents the chemical compositions of these steels in weight percentage. Thermo-Calc was utilized to calculate the following quantities:

(i) Solidus and liquidus temperatures

(ii) Quantities of phases precipitated throughout solidification and their evolution temperature

(iii) Phases of chemical composition at the end of the solidification process

(iv) Matrix chemical composition

(v) Nature of the present phase at 1100, 1150, 1200, and 1250°C

3.1. Solidus and Liquidus Temperatures of Investigated Steel. Figures 1 and 2 present the solidification path of SAE-AISI T1 steel and its variants. In these figures, the horizontal axis denotes the temperature, while the vertical one denotes the volume fraction of each phase. The closed circles in these figures indicate the solidus and liquidus temperatures of the investigated steels. In the case of vanadium-modified SAE-AISI T1 steel, the liquidus temperature is above 1450°C, but all the solidus temperatures are higher than 1275°C. On the other hand, in vanadium modified with extra carbon SAE-AISI T1 steel, the liquidus temperature is above 1400°C and the solidus temperature is above 1250°C. M_6C carbide solidus temperature decreases and MC carbide solidus temperature increases with a chemical composition of investigated steel variants. The results of the mentioned data were confirmed by the previous work [32].

3.2. Amount of Evolved Phases during Solidification. Figures 3–9 show the optical micrograph of the investigated steel in the as-cast condition. The volume fraction of evolved phases during solidification was measured by processing the optical micrograph and utilizing the ImageJ program, as shown in Figure 10. Additionally, the amount of different constituents was calculated theoretically using Thermo-Calc software. The total amount of the constituents utilizing Thermo-Calc software was given by volume percentage for ease of comparison with metallographic measurements. The volume fractions of different constituents are documented in Table 2.

3.2.1. Standard SAE-AISI T1 Steel. Figure 1(a) reports that the amount (volume fraction) of different carbides for standard SAE-AISI T1 steel at the end of solidification is approximately 22%. Moreover, the structure of standard SAE-AISI T1 steel at room temperature is the ferritic (martensitic) matrix with hard carbides (M_6C, $M_{23}C_6$, and MC). Figure 3 shows the optical micrographs of vanadium-modified SAE-AISI T1 steel in the as-cast condition. Table 2 represents the volume percentage of phases in standard SAE-AISI T1 steel.

For the solidification path of SAE-AISI T1 steel, M_6C evolved from the liquid phase at around 1324°C, consuming alloying elements and carbon needed to encourage another carbide's precipitation. Based on the Thermo-Calc calculation, MC carbides precipitated at about 1000°C because of solid-transformation reaction; furthermore, precipitation of MC at lower temperature was attributed to consuming carbon and other alloying elements from the matrix. The mentioned precipitation process leads to delay in the transformation process at lower temperature. Therefore, the metallographic examination of the investigated steel confirmed these results by studying many micrographs of SAE-AISI T1 steel. Figure 3 shows the optical micrograph of SAE-AISI T1 steel in the as-cast condition. Primary MC-carbide particles are observed as individual massive crystals, as a principle, in association with M_6C eutectic colonies. Consequently, MC carbide precipitated essentially at

Table 1: The chemical composition of investigating steel (as solidified).

Steel no.	Chemical composition, wt. %						
	C	Cr	W	V	Mo	Si	Fe
Standard T1 high-speed tool steel							
T1 high speed	0.78	4.15	17.95	1.1	0.48	0.19	Balance
Vanadium-modified T1 high-speed tool steel							
2V-13W	0.753	3.75	13.2	2.1	0.5	0.20	Balance
3V-8W	0.748	3.99	7.95	2.96	0.54	0.22	Balance
4V-3W	0.753	4.02	2.96	3.95	0.49	0.18	Balance
Vanadium with extra carbon-modified T1 high-speed tool steel							
2V-13W-HC	0.985	4.04	12.96	1.97	0.43	0.23	Balance
3V-8W-HC	1.22	3.89	8.06	2.88	0.51	0.17	Balance
4V-3W-HC	1.455	3.95	2.99	3.92	0.50	0.21	Balance

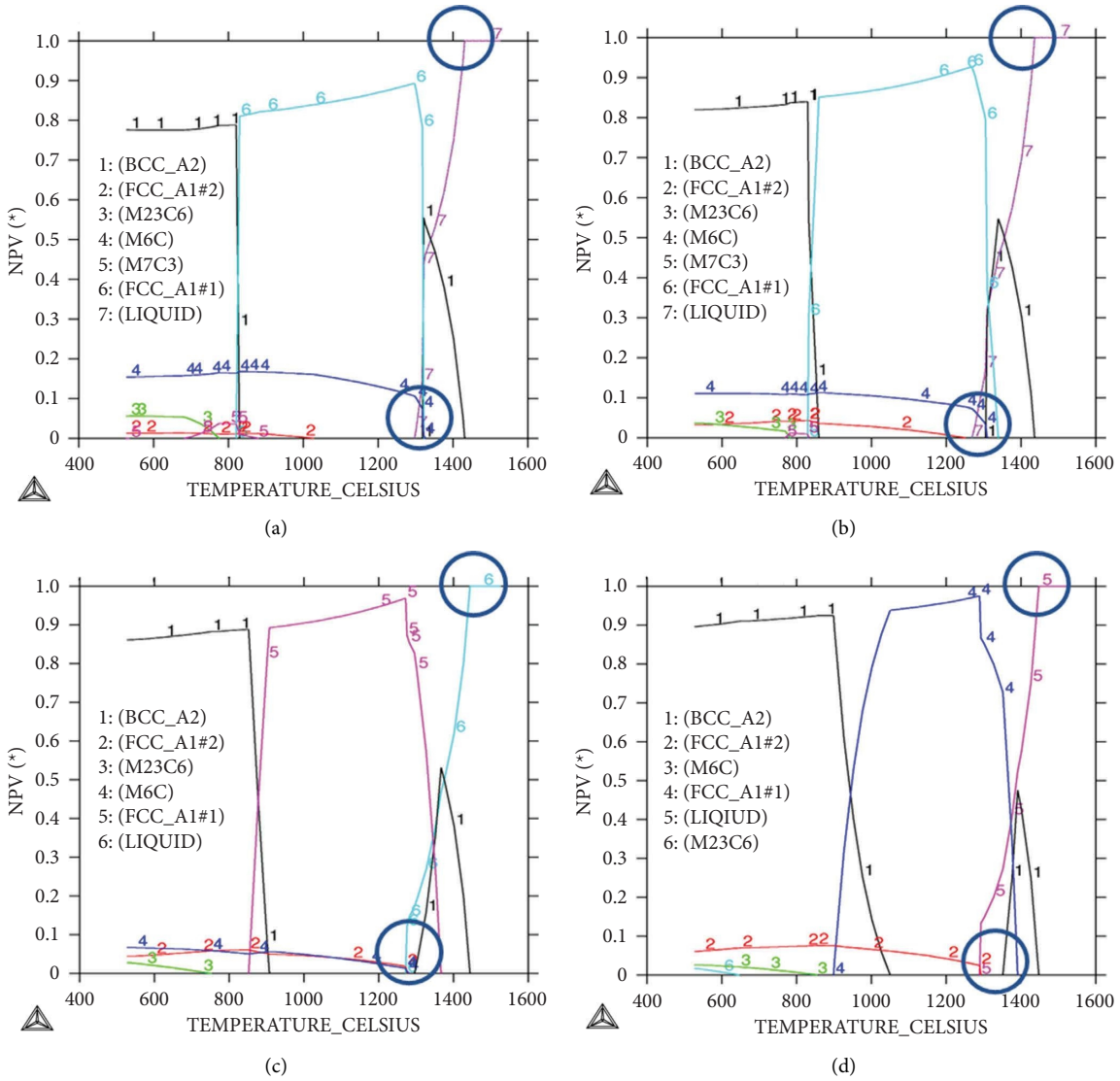

Figure 1: Solidification path of T1 high-speed tool steel and vanadium-modified variants. (a) 1V-18W; (b) 2V-13W; (c) 3V-8W; (d) 4V-3W.

high temperature. After that, M_6C carbide precipitated significantly at the final stage of the solid phase transformation process.

3.2.2. Vanadium-Modified SAE-AISI T1 Steel. Freezing paths of vanadium-modified SAE-AISI T1 steel and its variants show considerable changes in the phase amount

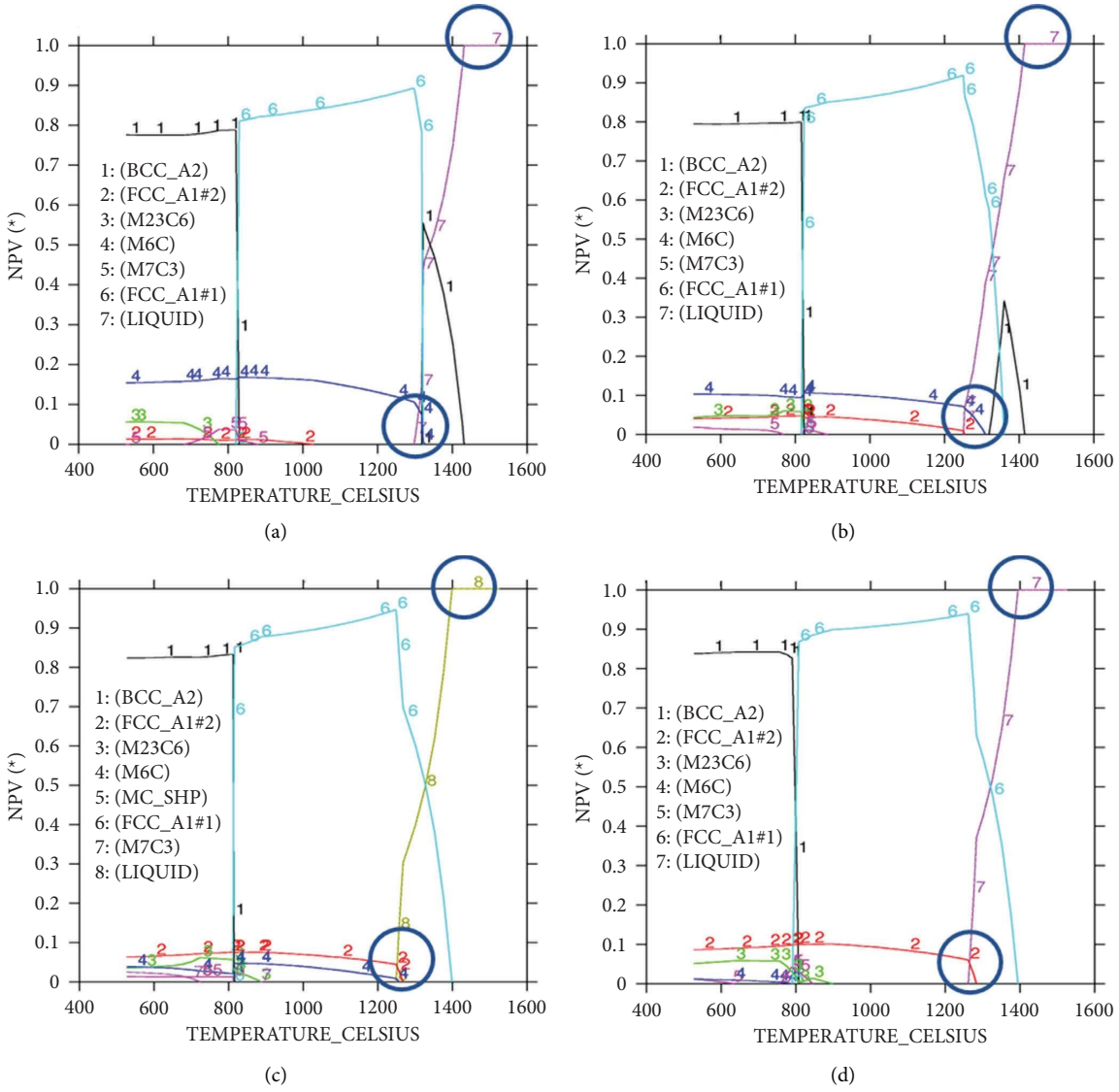

Figure 2: Solidification path of T1 high-speed tool steel and vanadium with extra carbon-modified variants. (a) 1V-18W; (b) 2V-13W-HC; (c) 3V-8W-HC; (d) 4V-3W-HC.

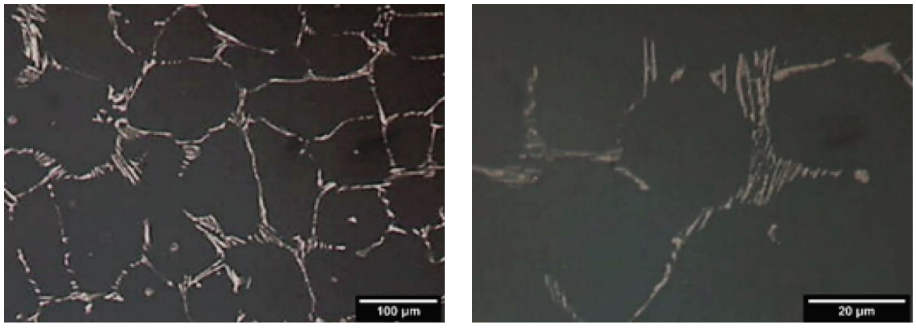

Figure 3: Microstructure of T1 high-speed tool steel in the as-cast condition.

and its evolution temperature compared with those of standard SAE-AISI T1 steel, as shown in Figure 1. Figure 1 shows a slight increase in liquidus temperature. In contrast, the solidus temperature of investigated vanadium-modified steel and its variants significantly decreased. Based on Thermo-Calc calculation and metallographic observation, Figure 1 presents that the structure of vanadium-modifiedhigh-speed tool steels is a mixture of carbides,

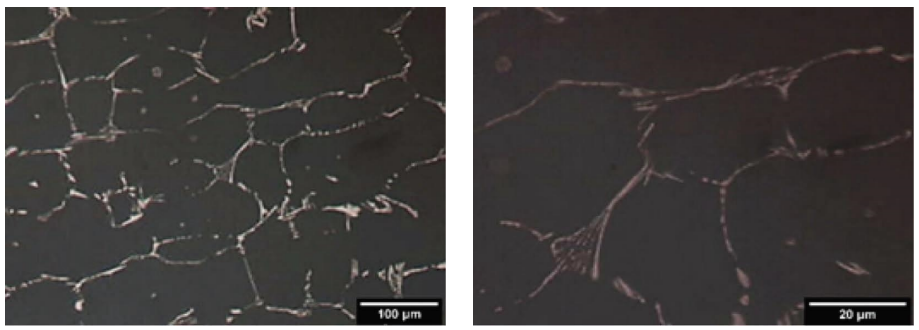

Figure 4: Microstructure of 2V-13W steel in the as-cast condition.

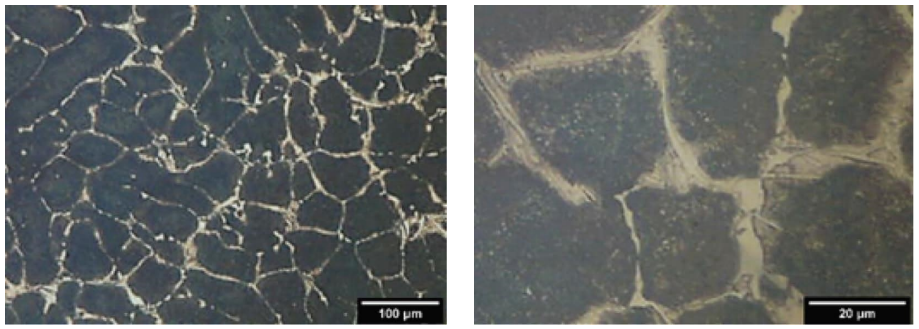

Figure 5: Microstructure of 3V-8W steel in the as-cast condition.

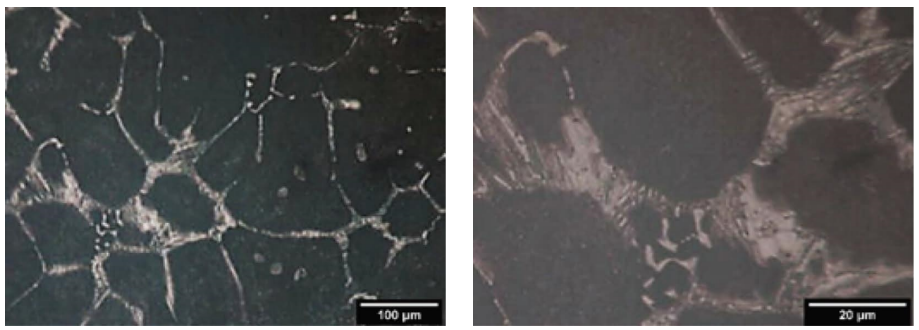

Figure 6: Microstructure of 4V-3W steel in the as-cast condition.

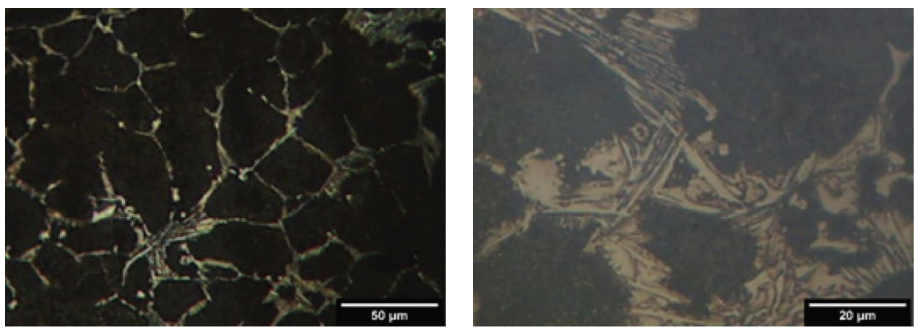

Figure 7: Microstructure of 2V-13W-HC steel in the as-cast condition.

mainly containing MC, M_6C, and $M_{23}C_6$ in the ferritic matrix. Furthermore, the microstructure of vanadium-modified steel is the same as that of standard SAE-AISI T1 steel but with a different amount. Figures 4–6 show the optical micrographs of vanadium-modified SAE-AISI T1 steel in the as-cast condition. Table 2 shows the magnitude

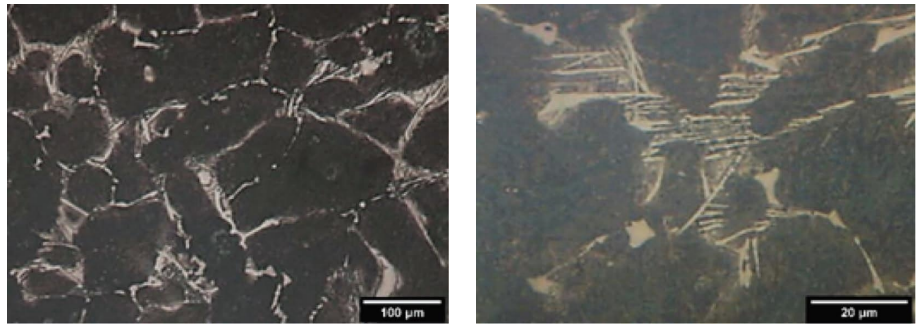

Figure 8: Microstructure of 3V-8W-HC steel in the as-cast condition.

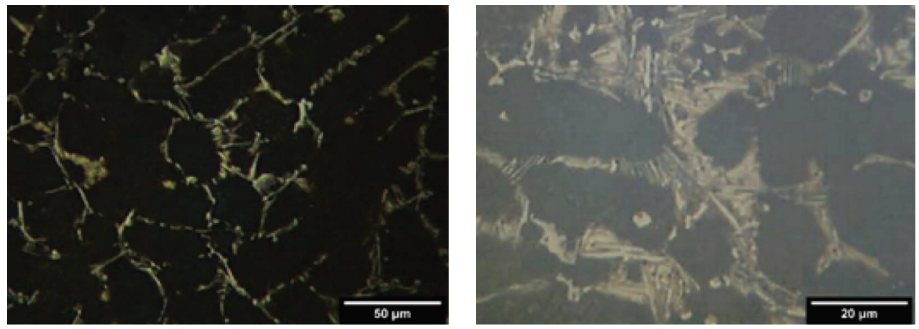

Figure 9: Microstructure of 4V-3W-HC steel in the as-cast condition.

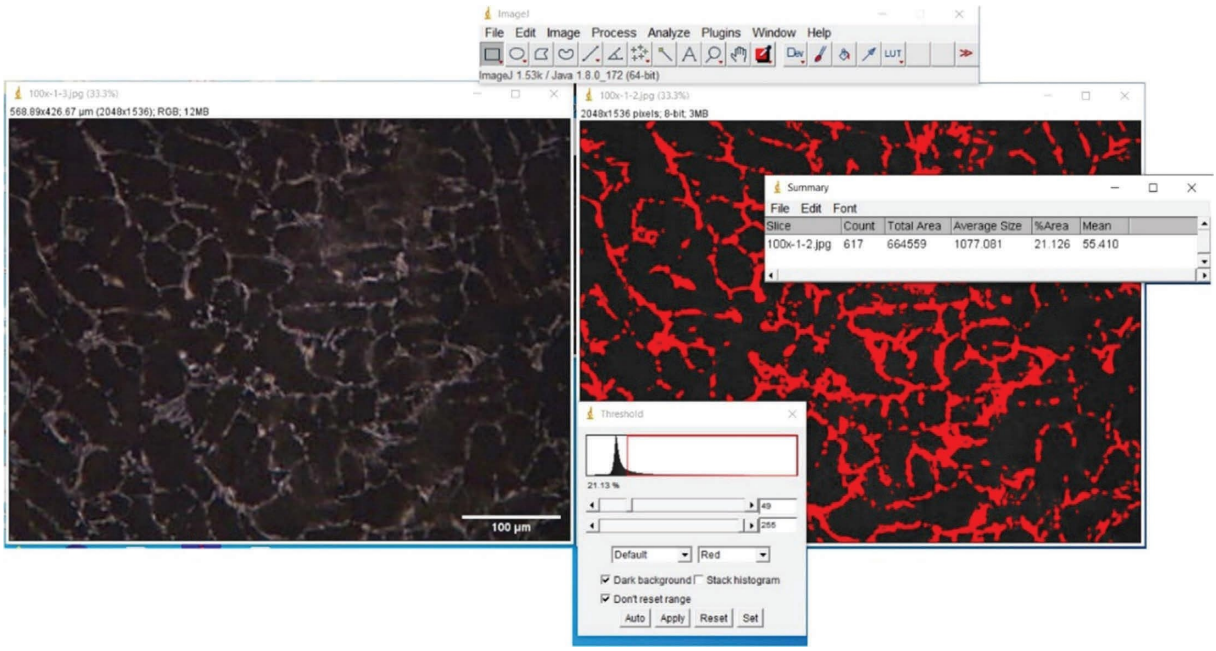

Figure 10: Utilizing the ImageJ program for calculating the total volume fraction of carbides.

of phases at room temperature for vanadium-modified steel. Additionally, Table 2 shows an increase in the amount of primary carbides (eutectic carbide and MC) instead of peritectic carbides (M_6C and $M_{23}C_6$) for different modified steels compared with that of standard SAE-AISI T1 steel. Moreover, Table 2 shows a reduction in the volume fraction of M_6C and $M_{23}C_6$ carbides in the order of 1V-18W, 2V-13W, 3V-8W, and 4V-3W steels, respectively.

In the previous work, the author concluded that vanadium additions associated with decreasing tungsten percentage promote the formation of MC carbide instead of M_6C and $M_{23}C_6$ carbides. This result was attributed to MC carbide favorable precipitation from relatively high vanadium and carbon contents in the molten steel alloys that consumed alloying elements required to precipitate M_6C and $M_{23}C_6$ carbides.

Table 2: Amount of the phase in the volume percent in T1 high-speed tool steel and its variant (as solidified).

Phases	State	Steel designation						
		Standard	Vanadium modified			Vanadium with extra carbon modified		
		1V-18W	2V-13W	3V-8W	4V-3W	2V-13W-HC	3V-8W-HC	4V-3W-HC
BCC (matrix)	Calculated	77.66	82.87	86.85	90.41	79.57	82.40	84.12
	Measured	79.19	83.54	87.21	89.65	80.81	83.79	84.52
MC	Calculated	1.37	3.30	4.80	6.61	4.18	6.57	8.89
	Measured	0.76	3.05	5.01	6.62	3.97	6.74	8.63
M_6C	Calculated	15.61	11.12	6.58	2.35	10.30	3.63	—
	Measured	15.48	11.32	6.35	3.73	10.71	3.83	—
$M_{23}C_6$	Calculated	5.48	2.64	2.10	0.69	4.77	3.86	0.66
	Measured	4.57	2.09	1.43	—	3.98	2.84	—
M_7C_3	Calculated	—	—	—	—	1.18	2.21	5.32
	Measured	—	—	—	—	—	—	5.08
MC-SHIP	Calculated	—	—	—	—	—	1.33	1.01
	Measured	—	—	—	—	—	—	—
Total carbides	Calculated	22.34	17.13	13.15	9.59	20.43	17.6	15.88
	Measured	20.81	16.46	12.79	10.36	18.66	13.41	13.61

∗ calculated: Thermo-Calc calculation; ∗ ∗ measured: microstructure measurement based on the ImageJ software.

3.2.3. Vanadium with Extra Carbon-Modified SAE-AISI T1 Steel. Frequently, the addition of carbon promotes the austenite phase stability of the investigated steel. Therefore, extra carbon associated with decreasing tungsten content leads to narrowing the ferrite (BCC) phase area and widening the austenite (FCC) phase area, as shown in Figure 2. The previous result assigned high carbon and vanadium with low tungsten magnitude in the melt. Furthermore, Figure 2 shows that the solidification path for vanadium with extra carbon-modified steel begins from the melt by FCC-austenite phase precipitation instead of the BCC-ferrite phase for both standard and vanadium-modified SAE-AISI T1 steel.

In addition, Figure 2 shows a significant decrease in liquidus and solidus temperatures for vanadium with extra carbon-modified SAE-AISI T1 steel. Table 2 shows the volume fraction of different phases present in vanadium with extra carbon-modified SAE-AISI T1 steel, which was determined by using Thermo-Calc software.

Figures 7–9 show the optical micrographs of vanadium-modified SAE-AISI T1 steel in the as-cast condition. Moreover, the structure of this steel group consists of primary carbides (MC and M_6C) and secondary carbides (M_7C_3, $M_{23}C_6$, and MC-SHIP) in a ferrite matrix. Figure 10 shows an example of utilizing the ImageJ program to calculate the carbide's total volume fraction. Differentiating between carbides and the matrix was performed by simple thresholding. Table 2 shows that the carbide volume fraction decreased gradually in the order of 2V-13W-HC and 3V-8W-HC steels, respectively, while M_6C carbide disappeared completely in 4V-3W-HC steel. Based on the metallographic examination and Thermo-Calc calculation, substituting tungsten by vanadium with extra carbon promotes the MC carbide type instead of M6C carbide and enhances secondary carbide precipitation, e.g., M_7C_3, $M_{23}C_6$, and MC-SHIP. Furthermore, secondary carbide precipitation enhancement is ascribed due to higher vanadium and carbon contents. Precipitation of secondary carbides results from solid phase transformation during solidification at a low temperature of around 800°C.

As aforementioned, decreasing the volume fraction of M_6C in the investigating steel, which is attributed to the introduction of vanadium with or without extra carbon, combined with a decrease in tungsten percentage in the investigating steel, leads to a change in the crystal structure of M_6C from Fe_3M_3C to Fe_4M_2C, which increases the mass of M_6C; however, the volume fraction of M_6C carbide decreases [38].

3.3. Chemical Composition of Different Constituents of the Investigated Steel. The solidified structure of the investigated steel consists of an alloyed ferritic matrix mixed with primary and secondary carbides. However, the chemical composition of different phases depends mainly on the solution's starting chemical composition at melting temperature. In addition, MC carbide has been considered a vanadium carbide dissolved in a limited magnitude of iron, tungsten, and chromium. M_6C carbide has been considered an iron-tungsten carbide that dissolves the minute magnitude of chromium and vanadium. However, $M_{23}C_6$ and M_7C_3 have been considered chromium-rich carbides [39].

Figures 11–13 show the scanning electron micrographs and EDX patterns of carbide particles and the matrix of the investigated steel in the as-cast condition. The group of tables based on thermodynamic calculation and EDX measurements was constructed for the investigated steel. Furthermore, Tables 3–8 show the chemical composition of different phases in weight percentage at the end of the solidification process for all steels under investigation. Therefore, from the previous section and Tables 3–8, it is expected that vanadium and vanadium with extra carbon modification will influence not only the starting temperature and the total amount of different phases but also their chemical compositions.

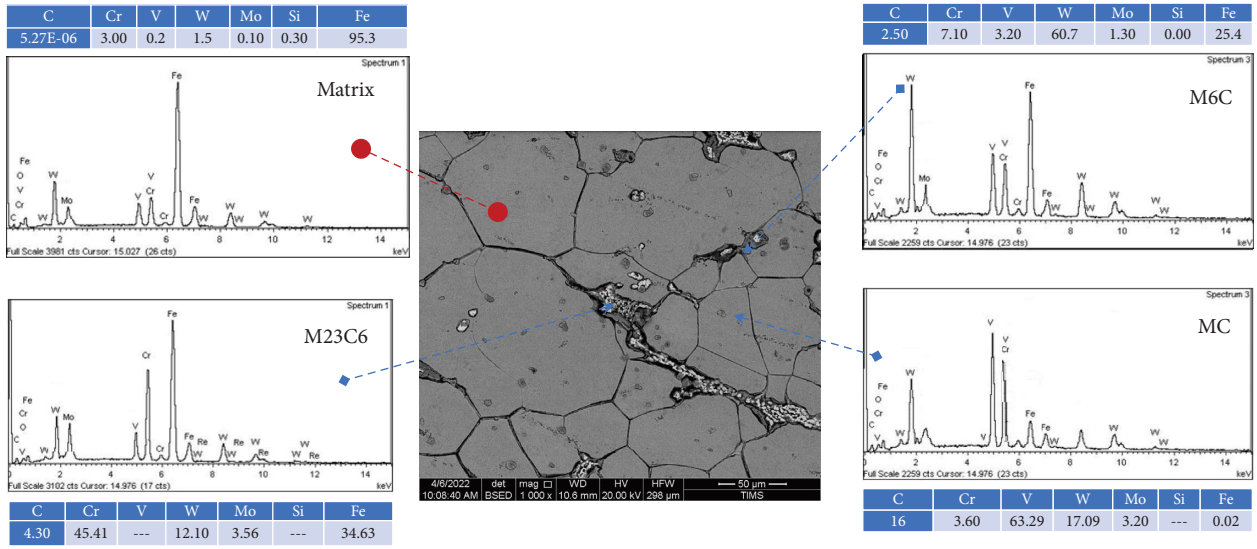

Figure 11: T1 high-speed tool steel.

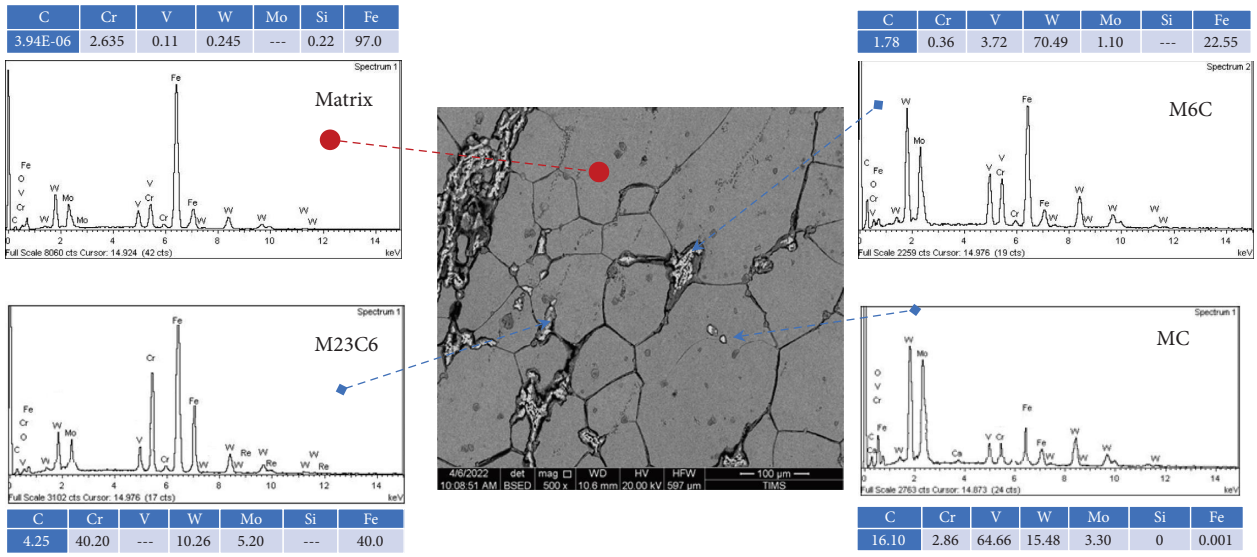

Figure 12: Vanadium-modified high-speed tool steel.

The authors carried out intensive studies to investigate the change in the phase chemical composition of the investigated steel, as summarized in the following parts.

3.3.1. MC Carbide. MC carbide has been identified as a face-centered cubic carbide and corresponds to a vanadium-rich carbide of composition ranging from VC to V_4C_3. Moreover, MC-carbide can dissolve many other alloying elements (tungsten, molybdenum, chromium, and iron) [39]. Table 3 shows that partially substituted tungsten by vanadium causes MC monocarbide to precipitate with a lower amount of tungsten, iron, and chromium. In addition, it has a slightly higher vanadium and molybdenum percentage than that of traditional SAE-AISI T1 steel. Furthermore, Table 3 shows that partially substituted tungsten by vanadium with extra carbon formed MC monocarbide with tungsten ranging from one and a half to three times more than tungsten in traditional SAE-AISI T1 steel. Moreover, vanadium with extra carbon-modified steel is composed of MC monocarbide with less vanadium but more molybdenum, chromium, and iron.

3.3.2. M_6C carbide. M_6C –carbide designated as tungsten or molybdenum-rich carbide matching the complex face-centered cubic carbide of the composition range from Fe_3W_3C to Fe_4W_2C or Fe_3W_3C to Fe_4Mo_2C in molybdenum high tool steel types. These carbides can solve some alloying elements, e.g., chromium, vanadium, and cobalt [38]. Table 4 shows the chemical composition of M_6C carbide of the investigated steel; moreover, Table 4 reported that vanadium-modified steels precipitated M6C carbide contained low tungsten content but dissolved higher vanadium and

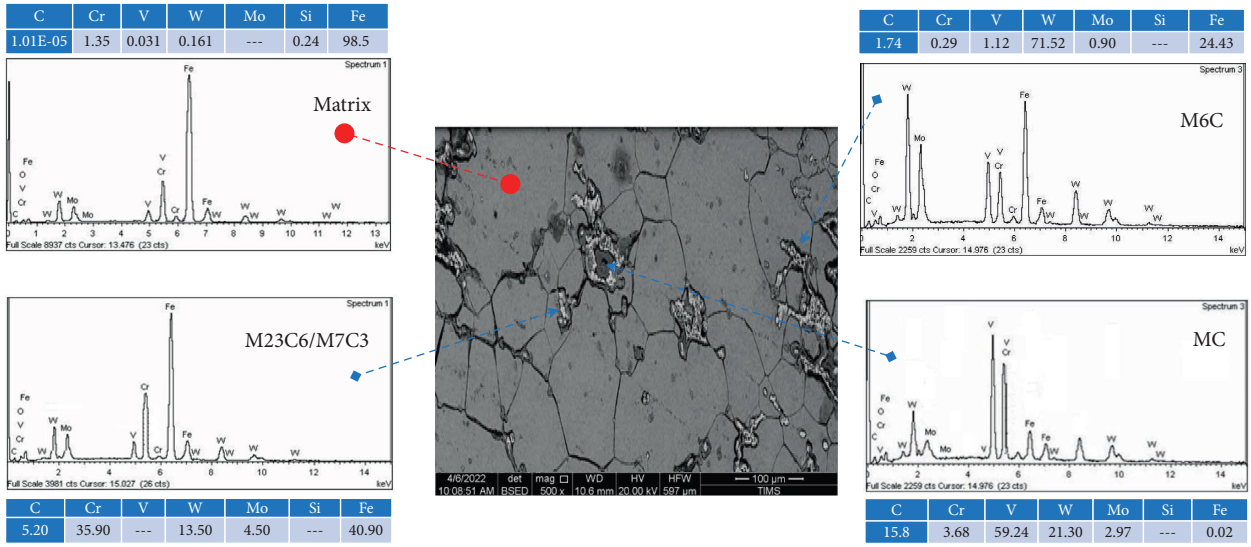

Figure 13: Carbon-vanadium-modified high-speed tool steel.

Table 3: Chemical composition of MC carbide for T1 high-speed tool steel and its different variants (as solidified).

Steel designation	State	Chemical composition, wt. %						
		C	Cr	V	W	Mo	Si	Fe
Standard T1 high-speed tool steel								
T1 high speed	Calculated	14.3	3.74	59.28	19.98	2.62	$5.16E-09$	0.08
	Measured	16	3.60	63.29	17.09	3.20	—	0.02
Vanadium-modified T1 high-speed tool steel								
2V-13W	Calculated	14.50	3.53	61.61	17.32	2.97	$3.80E-09$	0.07
	Measured	16.10	2.86	64.66	15.48	3.30	—	0.001
3V-8W	Calculated	14.80	3.18	64.9	13.69	3.37	$2.58E-09$	0.06
	Measured	16.10	2.42	67.02	13.15	3.51	—	0.001
4V-3W	Calculated	15.06	1.96	70.75	8.39	3.81	$1.39E-09$	0.04
	Measured	16.00	2.15	73.12	9.81	3.72	—	0.001
Vanadium with extra carbon-modified T1 high-speed tool steel								
2V-13 W-HC	Calculated	13.9	3.83	55.04	24.01	3.12	$6.35E-09$	0.1
	Measured	15.8	3.68	59.24	21.30	2.97	—	0.02
3V-8W-HC	Calculated	13.67	3.85	52.81	26.37	3.18	$6.73E-09$	0.11
	Measured	14.70	4.16	50.83	28.17	3.34	—	0.19
4V-3W-HC	Calculated	14.15	4.37	53.06	22.61	5.66	$1.04E-08$	0.15
	Measured	15.00	4.82	62.76	16.02	5.40	—	0.03

chromium contents in differentiation with traditional SAE-AISI T1 steel. Furthermore, in this case, the vanadium content ranges from one and a half to three and a half times more than the vanadium content in standard steel. On the other hand, in the case of vanadium with extra carbon-modified steel, M_6C carbide had slightly lower vanadium and chromium contents but had a higher amount of tungsten and iron than the vanadium content in standard steel.

3.3.3. $M_{23}C_6$. $M_{23}C_6$ carbide has been considered a chromium-rich carbide capable of dissolving some alloying elements (tungsten, molybdenum, and vanadium) [38]. The introduction of vanadium or vanadium with extra carbon accompanied with decreased tungsten content in the investigated steel, however, leads to a change in the crystal structure of M_6C from Fe_4M_2C to $Fe_{21}M_2C_6$ [37], as reported in Table 5. Table 5 presents the chemical composition of $M_{23}C_6$ in the investigated steel. Also, Table 5 shows that $M_{23}C_6$ carbide precipitated in vanadium-modifiedhigh-speed steel with higher chromium and molybdenum contents than those in SAE-AISI T1 steel. Moreover, $M_{23}C_6$ carbide precipitating in the case of vanadium with extra carbon-modifiedhigh-speed steel contained lower chromium and molybdenum contents than those in traditional SAE-AISI T1 steel.

3.3.4. M_7C_3. M_7C_3 carbide is a chromium carbide capable of dissolving traces of other elements, e.g., vanadium, iron, and tungsten [38]. The solidification path of the investigating steel demonstrates that M_7C_3 carbide disappeared from the final structure in both standard and vanadium-modified SAE-AISI T1 steels. The previous result attributed to most

Table 4: Chemical composition of M_6C carbide for T1 high-speed tool steel and its different variants (as solidified).

Steel designation	State	Chemical composition, wt. %						
		C	Cr	V	W	Mo	Si	Fe
Standard T1 high-speed tool steel								
T1 high speed	Calculated	1.81	1.37	1.86	68.02	1.23	0.00	25.70
	Measured	2.50	7.10	3.20	60.7	1.30	0.00	25.4
Vanadium-modified T1 high-speed tool steel								
2V-13W	Calculated	1.82	1.44	2.40	67.42	1.65	—	25.27
	Measured	1.78	0.36	3.72	70.49	1.10	—	22.55
3V-8W	Calculated	1.85	1.53	3.53	66.09	2.48	—	24.52
	Measured	1.81	0.37	5.67	69.26	2.70	—	20.19
4V-3W	Calculated	1.92	1.20	6.96	62.36	4.64	—	22.93
	Measured	1.88	0.33	9.18	66.91	5.20	—	16.50
Vanadium with extra carbon-modified T1 high-speed tool steel								
2V-13W-HC	Calculated	1.81	1.24	1.27	68.19	1.20	—	26.29
	Measured	1.74	0.29	1.12	71.52	0.90	—	24.43
3V-8W-HC	Calculated	1.81	1.16	1.05	68.29	1.12	—	26.57
	Measured	1.75	0.25	0.62	71.33	0.50	—	25.55

Table 5: Chemical composition of $M_{23}C_6$ carbide for T1 high-speed tool steel and its different variants (as solidified).

Steel designation	State	Chemical composition, wt. %						
		C	Cr	V	W	Mo	Si	Fe
Standard T1 high-speed tool steel								
T1 high speed	Calculated	4.85	41.04	0.01	14.32	4.22	—	35.56
	Measured	4.30	45.41	—	12.10	3.56	—	34.63
Vanadium-modified T1 high-speed tool steel								
2 V- 13W	Calculated	4.87	43.60	0.01	13.26	5.39	---	32.87
	Measured	4.25	40.20	—	10.26	5.20	—	40.09
3V-8W	Calculated	4.92	47.59	0.01	11.35	7.42	—	28.71
	Measured	4.78	44.2	—	9.51	7.20	—	34.31
4V-3W	Calculated	—	—	—	—	—	—	—
	Measured	—	—	—	—	—	—	—
Vanadium with extra carbon-modified T1 high-speed tool steel								
2V-13W-HC	Calculated	4.83	36.89	0.01	14.45	3.99	—	39.83
	Measured	5.20	35.90	—	13.50	4.50	—	40.90
3V-8W-HC	Calculated	4.83	34.73	0.01	14.62	3.73	—	42.09
	Measured	5.15	30.90	0.00	11.61	4.30	—	48.04
4V-3W-HC	Calculated	—	—	—	—	—	—	—
	Measured	—	—	—	—	—	—	—

Table 6: Chemical composition of M_7C_3 carbide for T1 high-speed tool steel and its different variants (as solidified).

Steel designation	State	Chemical composition, wt. %						
		C	Cr	V	W	Mo	Si	Fe
Vanadium with extra carbon-modified T1 high-speed tool steel								
2V-13W-HC	Calculated	8.70	61.67	5.12	2.60	0.39	—	21.51
	Measured	8.93	68.81	4.50	0.66	0.20	—	16.902
4V-3W-HC	Calculated	8.68	55.09	3.43	1.82	0.65	—	30.33
	Measured	8.70	58.11	4.16	2.28	0.50	—	26.25

Table 7: Chemical composition MC-SHIP carbide for T1 high-speed tool steel and its different variants (as solidified).

Steel designation	State	Chemical composition, wt. %						
		C	Cr	V	W	Mo	Si	Fe
Vanadium with extra carbon-modified T1 high-speed tool steel								
3V-8W-HC	Calculated	6.20	—	—	92.59	1.21	—	—
	Measured	6.00	—	—	91.70	2.3	—	—
4V-3W-HC	Calculated	6.27	—	—	91.24	1.21	—	—
	Measured	5.80	—	—	91.10	3.1	—	—

Table 8: Chemical composition of the matrix for T1 high-speed tool steel and its different variants (as solidified).

Steel designation	State	Chemical composition, wt. %						
		C	Cr	V	W	Mo	Si	Fe
Standard T1 high-speed tool steel								
T1 high speed	Calculated	$1.71E-03$	2.95	0.11	0.87	0.06	0.28	95.73
	Measured	$5.27E-06$	3.00	0.2	1.5	0.10	0.30	95.3
Vanadium-modified T1 high-speed tool steel								
2 V-13W	Calculated	$1.43E-03$	3.38	0.15	0.94	0.08	0.25	95.19
	Measured	$3.94E-06$	2.635	0.11	0.245	—	0.22	97.011
3V-8W	Calculated	$1.10E-03$	4.14	0.23	1.05	0.12	0.23	94.23
	Measured	$3.13E-06$	3.309	0.166	0.27	0.15	0.21	96.255
4V-3W	Calculated	$5.03E-04$	4.20	0.50	1.17	0.23	0.22	93.69
	Measured	$2.43E-06$	4.272	0.278	0.288	0.27	0.22	95.16
Vanadium with extra carbon-modified T1 high-speed tool steel								
2V-13W-HC	Calculated	$2.30E-03$	2.30	0.07	0.76	0.06	0.26	96.55
	Measured	$1.01E-05$	1.35	0.031	0.161	—	0.24	98.46
3V-8W-HC	Calculated	$2.70E-03$	2.02	0.06	0.71	0.05	0.24	96.91
	Measured	$1.84E-05$	0.94	0.015	0.125	—	0.21	98.92
4V-3W-HC	Calculated	$4.54E-03$	1.34	0.03	0.35	0.05	0.23	97.99
	Measured	$3.64E-03$	1.65	0.049	0.539	—	0.22	97.75

of the alloying elements consumed in evolution of MC, M_6C, and $M_{23}C_6$ carbides in addition to a high-alloyed matrix. Table 6 presents the M_7C_3 carbide's chemical composition calculated by using Thermo-Calc, compared with that of EDX measurements. Additionally, in the case of vanadium with extra carbon-modified steel, Table 6 reveals that M_7C_3 carbide contains higher vanadium content than that in standard steel; otherwise, it contains lower chromium, iron, and tungsten contents.

Based on the solidification path of vanadium with extra carbon-modified steel, the authors concluded that the introduction of vanadium and carbon accompanied by decreased tungsten content increases the formation of M_7C_3 carbide. M_7C_3 carbide precipitated from solid-solid transformation reaction at a temperature of around 800°C. Consequently, M_7C_3 carbide has been recognized as a secondary carbide.

3.3.5. MC-SHIP Carbides. Due to extraordinary carbon and vanadium contents for the investigated steel, MC-SHIP carbides precipitated according to solid-solid transformation reaction at low temperature. Table 7 shows that MC-SHIP (tungsten carbide) did not appear in standard and vanadium-modified SAE-AISI T1 steels but was present with a low amount in (3V-8W-HC) and (4V-3W-HC) extra carbon modified steel, respectively.

3.3.6. Matrix. Table 8 presents the matrix chemical composition of the investigated steel. Therefore, it reports that the matrix's chemical composition of vanadium-modified SAE-AISI T1 steel contained higher content of alloying elements than that of standard SAE-AISI T1 steel. In addition, Table 8 shows that the matrices of vanadium-modified steel contained three times more vanadium content and two times more chromium content than those of standard SAE-AISI T1 steel. In the case of vanadium-modified steel, compared with those of standard SAE-AISI T1 steel, the mentioned results are attributed to fewer precipitated carbides. Table 8 illustrates that the matrices of vanadium with extra carbon-modified SAE-AISI T1 steel contained a lower magnitude of alloying elements than that of standard steel. The mentioned results are attributed to consuming alloying elements from the molten steel to promote carbide precipitation, which contained higher carbon, vanadium, and tungsten contents than those of standard SAE-AISI T1 steel.

3.4. Influence of Austenitizing Temperature on the Amount and Chemical Composition of the Matrix and Carbides. Thermo-Calc software was employed for differentiating between types of carbides. Excellent agreement is found between the experiment and calculated data when the database is optimized on experimental results bases represented in this work. In particular, the changes in the chemical composition of the matrices and the recognized carbides (MC, M_6C, $M_{23}C_6$, M_7C_3, and MC-SHIP) chemical composition.

A series of constructed figures analyzed the effects of tungsten partial replacement by vanadium or vanadium with extra carbon on the volume fraction and chemical composition of phases with changes in the austenitizing temperature. Figures 14–16 show the volume fraction and chemical compositions of MC and M_6C carbide particles, while Figure 17 includes the volume fraction of gamma-austenite in the temperature range from 1000°C to 1250°C for all investigated steel. In addition, these figures show a slight change in the carbide's chemical composition, with an increased austenitizing temperature that encouraged the carbide dissolution process for different investigated steel. These figures confirmed that the dissolution of carbides through heating promotes gamma-austenite formation with higher alloying elements. Previous work stated that the matrix composition is of positive importance because it determines the starting requirement for secondary carbide precipitation. Indeed,

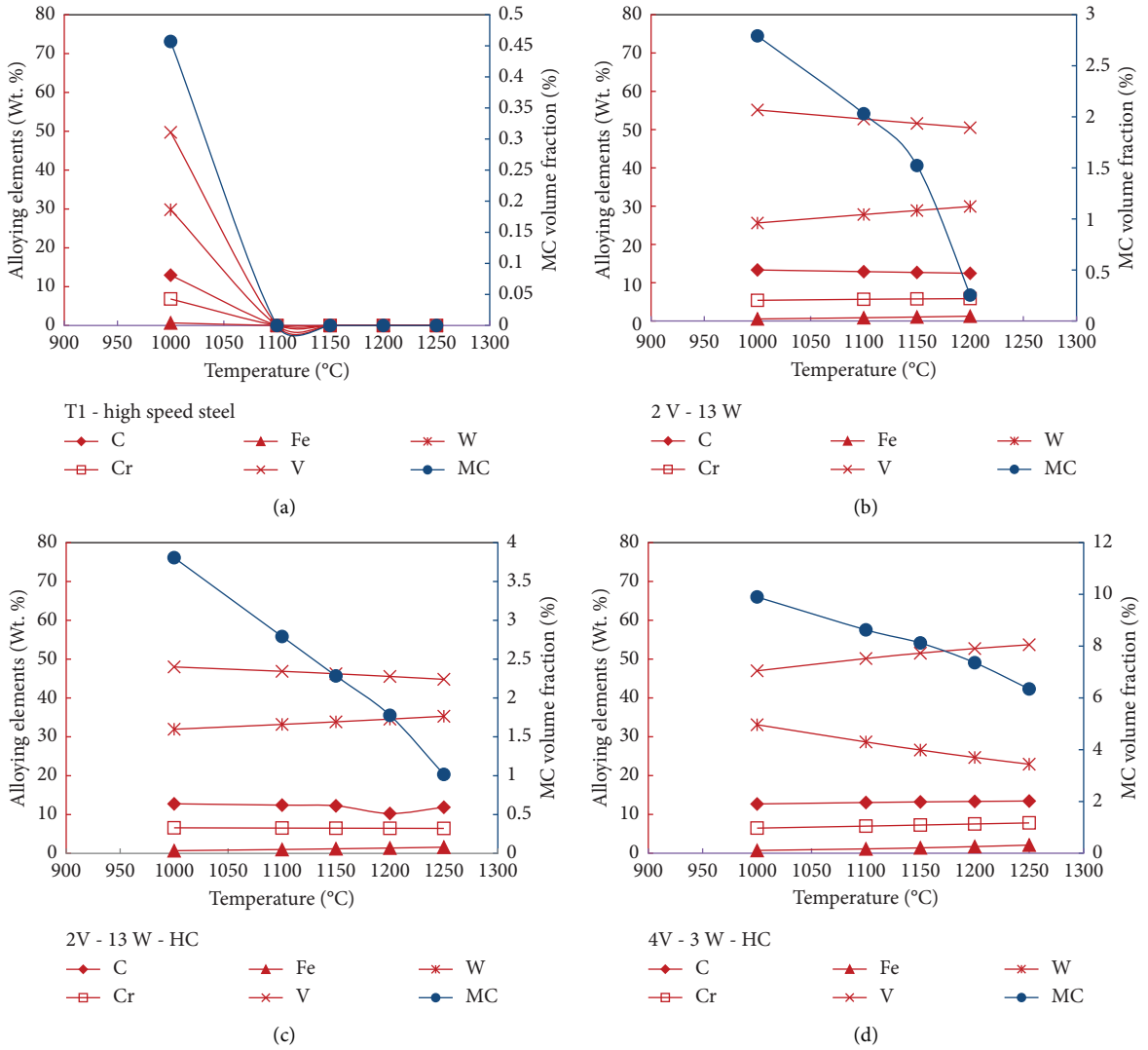

Figure 14: Chemical composition and the volume fraction of MC carbide presented in investigating steel at different austenitization temperatures. (a) T1 high-speed steel, (b) 2V-13W, (c) 2V-13W-HC, and (d) 4V-3W-HC.

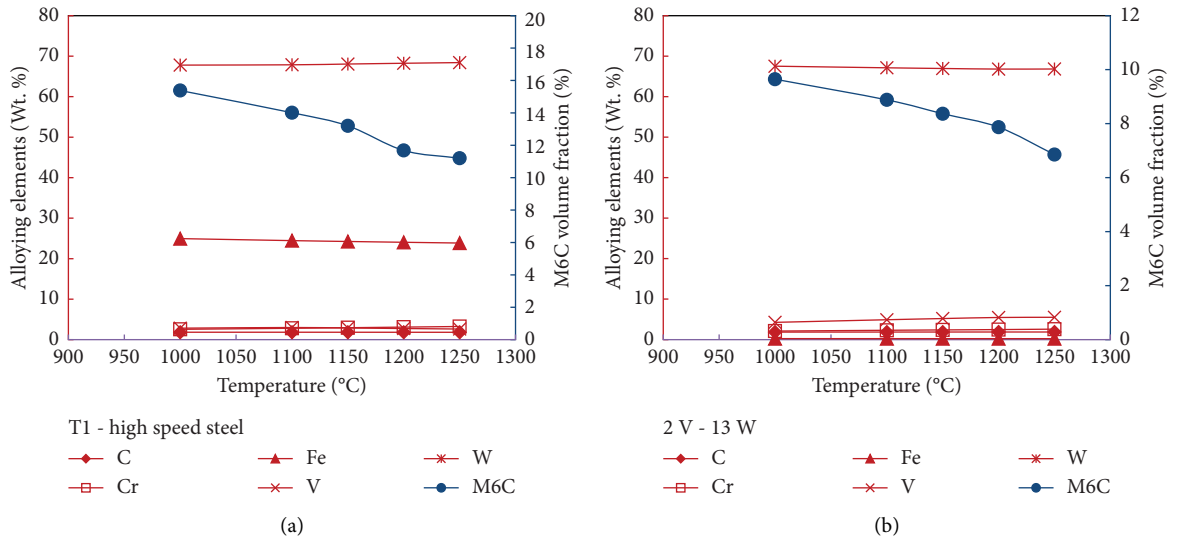

Figure 15: Continued.

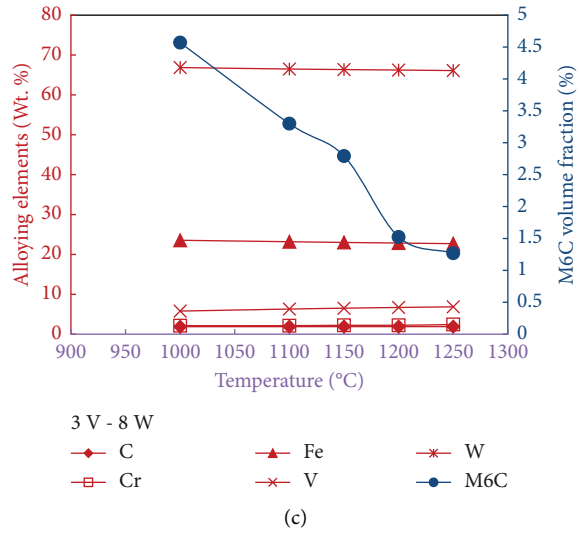

FIGURE 15: Chemical composition and the volume fraction of M_6C carbide presented in vanadium-modified steel at different austenitization temperatures. (a) T1 high-speed steel, (b) 2V-13W, and (c) 3V-8W.

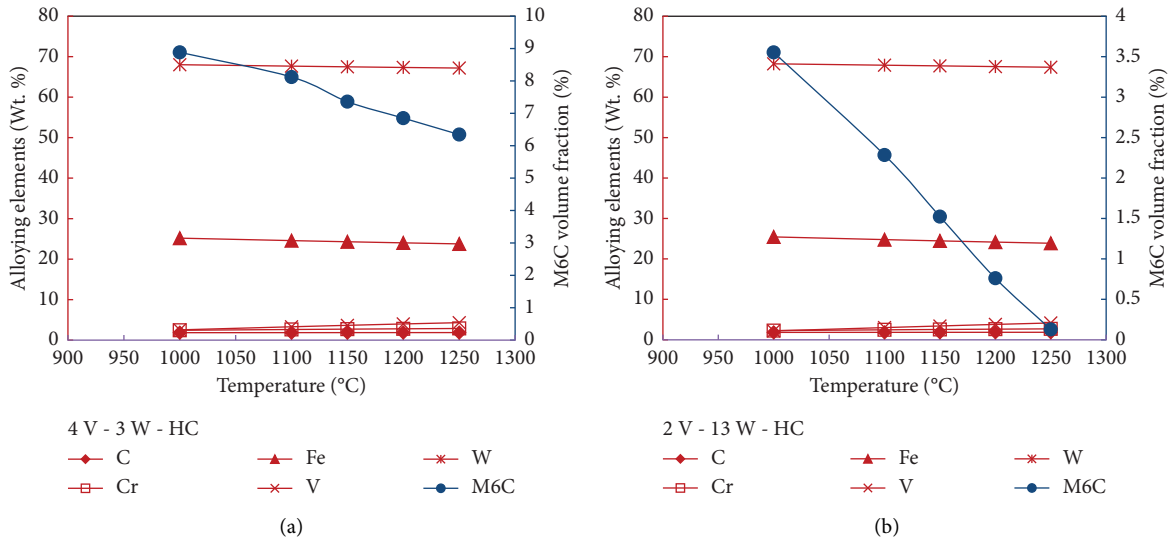

FIGURE 16: Chemical composition and the volume fraction of M_6C carbide presented in vanadium with extra carbon-modified steel at different austenitization temperatures. (a) 2V-13W-HC and (b) 3V-8W.

the matrix composition controls the technological properties of the investigated steel, such as wear, hardness, and secondary hardness [40].

From the previous work, the author concluded a non-significant change in the carbide's chemical composition, especially MC and M_6C, with the test temperature range. Indeed, carbide dissolution through heating increases the alloying element's content and promotes the formation of FCC-austenite with a higher alloying element. Since the solution annealing treatment of the investigated steel is carried out at 1230°C, different phases should offer a state approaching the thermodynamic equilibrium. Therefore, austenite and carbide compositions are used as a reasonable basis for differentiation in the following section.

3.5. Heat Treatment of the Investigated Steel. Concurrently, Figures 1 and 2 show that M_6C and $M_{23}C_6$ carbide particles in the investigating steel dissolved completely and were soluble in austenite through heating; however, MC vanadium base carbide dissolved harder. Dissolution of these carbides through heating leads to a high-alloyed austenitic matrix formation. Therefore, the microstructure is converted into martensite and retained austenite during the hardening-quenching process. Previous work affirmed that the matrix's chemical composition is the critical factor, affecting the amount and chemical composition of the final structure. However, the microstructure of full heat treatment steel mainly consists of tempered martensite, primary carbides (MC and M_6C), and secondary carbides ($M_{23}C_6$, M_7C_3, and MC-SHIP).

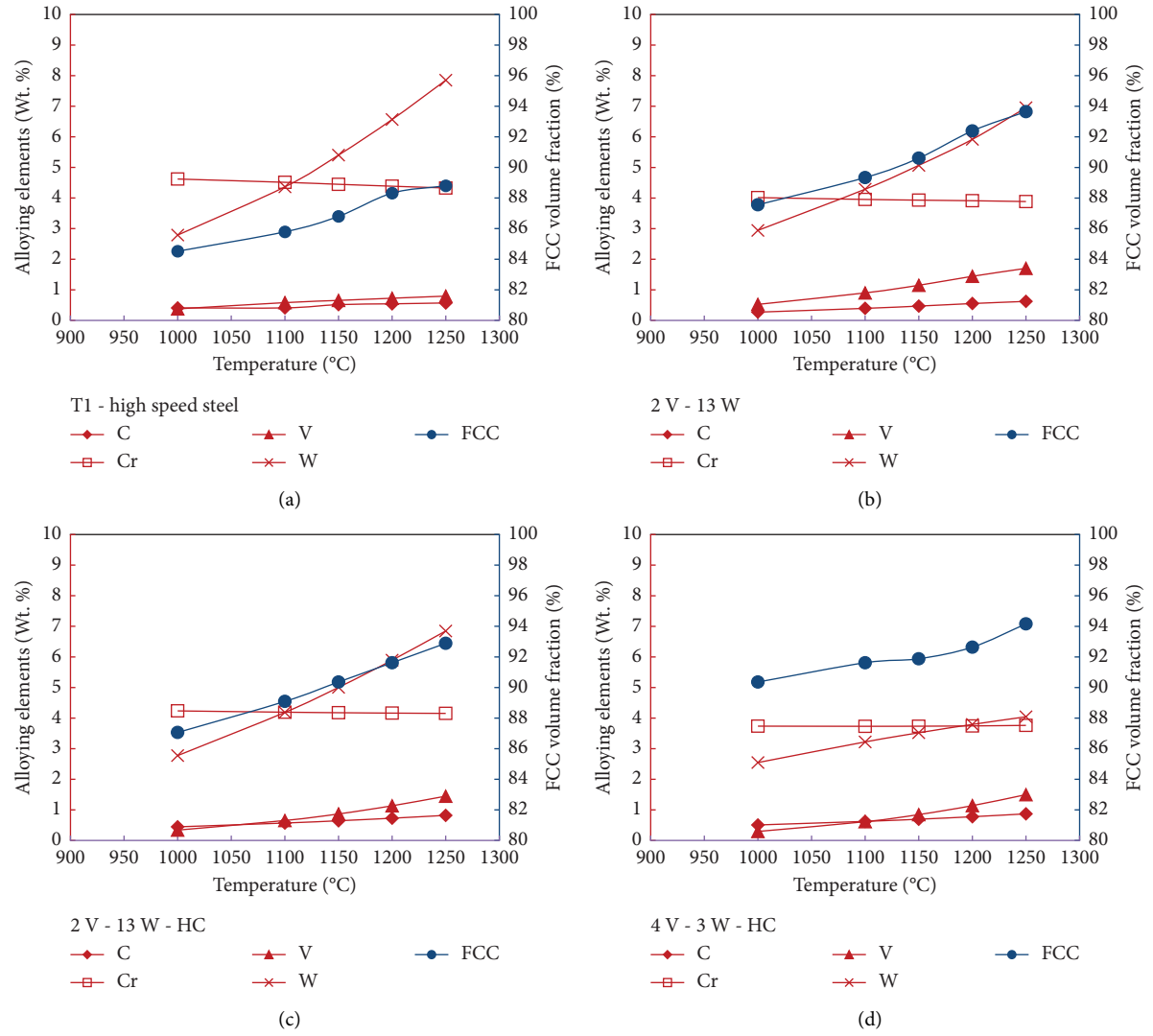

Figure 17: Chemical composition and the volume fraction of the austenitic (FCC) matrix presented in investigating steel at different austenitization temperatures. (a) T1 high-speed steel, (b) 2V-13W, (c) 2V-8W-HC, and (d) 4V-3W-HC.

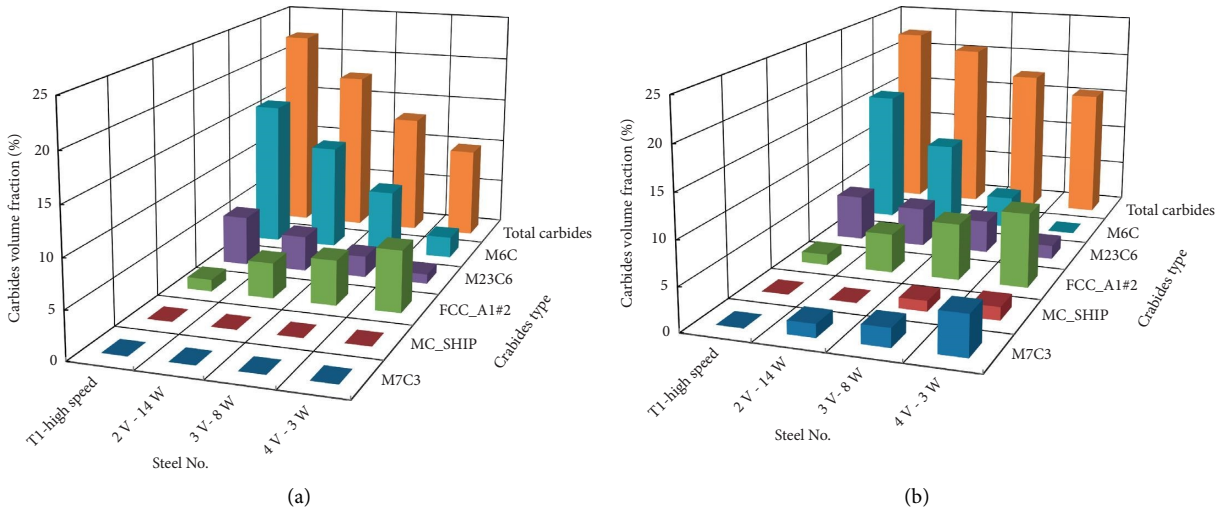

Figure 18: Carbide volume fraction for heat-treated investigating steel. (a) Vanadium-modified steel; (b) vanadium with extra carbon-modified steel.

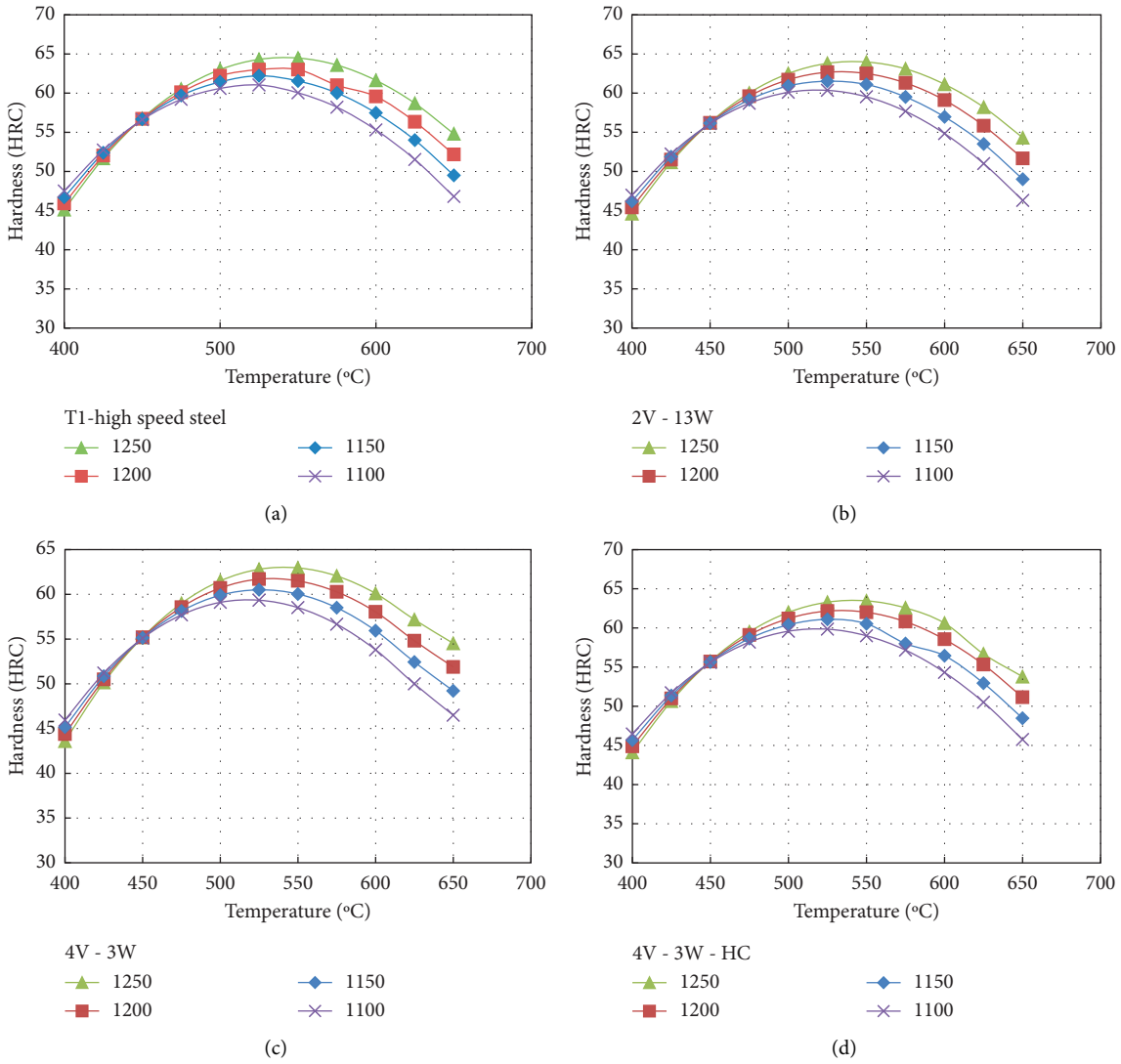

Figure 19: Hardness versus tempering temperature for investigating steel at different austenitization temperatures. (a) T1 high-speed steel, (b) 2V-13W, (c) 4V-3W, and (d) 4V-3W-HC.

Table 9: Secondary hardening temperature and hardness values of investigating steels.

Designation	Austenitization temperature							
	1100°C		1150°C		1200°C		1250°C	
	T^*	H^{**}	T	H	T	H	T	H
Standard T1 high-speed tool steel								
1V-18W	525	61	525	62	550	64	550	65
Vanadium-modified T1 high-speed tool steel								
2V-13W	525	60	525	62	525	63	525	64
3V-8W	525	60	525	61	550	62	525	63
4V-3W	525	59	525	61	525	62	550	63
Vanadium with extra carbon-modified T1 high-speed tool steel								
2V-13W–HC	525	60	525	64	525	65	550	66
3V-8W-HC	525	63	525	64	550	65	550	67
4V-3W-HC	525	64	550	65	525	66	550	67

$^*T$: tempering temperature; $^{**}H$: hardness value.

3.6. Secondary Hardening. Figure 18 presents the volume fraction of the carbide's full heat treatment of the investigated steel as an example; moreover, Figure 18 shows that vanadium-modified steel contained approximately the same quantity of secondary carbides compared with that of standard steel. Vanadium with extra carbon modification promoted the higher volume fraction of secondary carbides to let them precipitate after full heat treatment due to matrix alloying elements and excess carbon content.

Figure 19 presents an example of the effect of hardening (austenitizing) and tempering temperature variation on hardness values. Also, Figure 19 shows that an increase in hardening temperature leads to increased hardness after the tempering process. Table 9 shows the optimum tempering temperature and accompanying secondary hardening value of the investigated steels. Concurrently, Table 9 and Figure 19 show that the secondary hardening temperature is almost the same for all investigated steel. In the case of vanadium-modified steel, the secondary hardening value is lower or equal to that of standard steel. In the case of vanadium with extra carbon-modified steel, the secondary hardening value is higher than that of SAE-AISI T1 standard steel. Therefore, the excellent secondary hardening value was verified for steel containing higher tungsten and lower vanadium content with or without extra carbon. These results are attributed to higher total carbides and higher amounts of secondary carbides with higher alloying elements.

4. Conclusions

The obtained conclusions are listed as follows:

(1) The thermodynamic computations of phase equilibrium for modified SAE-AISI T1 steel showed that the findings are in remarkable agreement with the results of measurement for the solidification path, the volume fraction, and the compositions of constituents of the investigated steel. Moreover, understanding particular solidification characteristics that are only hypothetical is specified by the computation.

(2) The experimental findings for the variations in the chemical composition of the matrix and eutectic carbides precipitated, e.g., MC, M_6C, $M_{23}C_6$, and M_7C_3, agree well with the calculated findings.

(3) Tungsten replacement by vanadium with and without extra carbon in traditional SAE-AISI T1 steel encourages MC carbide formation instead of M_6C carbide. MC carbide precipitating in vanadium with extra carbon contains more carbon, chromium, and tungsten content but less vanadium content, compared with those in vanadium-modified steel.

(4) Vanadium with extra carbon-modified steel contained more precipitated M_6C carbides and gamma-austenite, which dissolved more alloying elements than vanadium modified steels.

(5) MC and M_6C carbides offer a state approaching the thermodynamic equilibrium because their chemical composition did not change significantly in the tested solid solution temperature range.

(6) Hardness measurements emphasized that modified steel is a promising material for its use as a tooling material with low tungsten content and, in turn, produces cutting-tool materials with economical cost.

Data Availability

No underlying data were collected or produced in this study.

Conflicts of Interest

The authors declare that they have no conflicts of interest.

Acknowledgments

The authors would like to acknowledge the Center of Excellence for Research in Engineering Materials (CEREM), Deanship of Scientific Research, King Saud University. The steel samples used in this study were designed and produced at the pilot plant of the Advanced Melting Technology Unit, Central Metallurgical Research and Development Institute "CMRDI," Egypt.

References

[1] T. P. Rich, J. G. Orbison, R. S. Duncan, P. G. Olivero, and R. H. Peterec, "The effect of hot isostatic pressing on crack initiation, fatigue, and mechanical properties of two cast aluminum alloys," *Journal of Materials Engineering and Performance*, vol. 8, no. 3, pp. 315–324, 1999.

[2] V. Arnhold, D. Duda, and R. Wahling, "Cutting tools from P/M high-speed steels," *Powder Metallurgy International*, vol. 21, no. 2, pp. 67–74, 1989.

[3] L. A. Dobrzański, M. Adamiak, and G. E. D'Errico, "Relationship between erosion resistance and the phase and chemical composition of PVD coatings deposited onto high-speed steel," *Journal of Materials Processing Technology*, vol. 92, pp. 184–189, 1999.

[4] L. A. Dobrzański and M. Adamiak, "Structure and properties of the TiN and Ti (C, N) coatings deposited in the PVD process on high-speed steels," *Journal of Materials Processing Technology*, vol. 133, no. 1-2, pp. 50–62, 2003.

[5] L. A. Dobrzański and M. Adamiak, "The structure and properties of PVD coated PM high-speed steels," in *Key Engineering Materials*, vol. 189, pp. 381–387, Trans Tech Publications Ltd, 2001.

[6] L. A. Dobrzański, A. Zarychta, and M. Ligarski, "High-speed steels with addition of niobium or titanium," *Journal of Materials Processing Technology*, vol. 63, no. 1-3, pp. 531–541, 1997.

[7] F. Deirmina, N. Peghini, B. AlMangour, D. Grzesiak, and M. Pellizzari, "Heat treatment and properties of a hot work tool steel fabricated by additive manufacturing," *Materials Science and Engineering A*, vol. 753, no. 753, pp. 109–121, 2019.

[8] F. Pan, P. Ding, A. Tang, M. Hirohashi, Y. Lu, and D. V. Edmonds, "Carbides in high-speed steels containing

silicon," *Metallurgical and Materials Transactions A*, vol. 35, no. 9, pp. 2757–2766, 2004.

[9] L. A. Dobrzański and M. Ligarski, "Role of Ti in the W-Mo-V high-speed steels," *Journal of Materials Processing Technology*, vol. 64, no. 1-3, pp. 101–116, 1997.

[10] H. Halfa, "Characterization of electroslag remelted super hard high speed tool steel containing niobium," *Steel Research International*, vol. 84, no. 5, pp. 495–510, 2013.

[11] H. F. Fischmeister, S. Karagöz, and H. O. Andren, "An atom probe study of secondary hardening in high speed steels," *Acta Metallurgica*, vol. 36, no. 4, pp. 817–825, 1988.

[12] H. O. Andrén, S. Karagöz, C. Guangjun, L. Lundin, and H. Fischmeister, "Carbide precipitation in chromium steels," *Surface Science*, vol. 246, no. 1-3, pp. 246–251, 1991.

[13] S. Karagöz and H. F. Fischmeister, "Cutting performance and microstructure of high speed steels: contributions of matrix strengthening and undissolved carbides," *Metallurgical and Materials Transactions A*, vol. 29, no. 1, pp. 205–216, 1998.

[14] A. K. Sinha, *Physical Metallurgy Handbook*, McGraw-Hill, New York, NY, USA, 2003.

[15] E. Keehan, L. Karlsson, H. O. Andrén, and H. K. D. H. Bhadeshia, "Influence of carbon, manganese, and nickel on microstructure and properties of strong steel weld metals: part 3–increased strength resulting from carbon additions," *Science and Technology of Welding & Joining*, vol. 11, no. 1, pp. 19–24, 2006.

[16] J. Kasinska and B. Kalandyk, "Effects of rare earth metal addition on wear resistance of chromium-molybdenum cast steel," *Archives of Foundry Engineering*, vol. 17, no. 3, pp. 63–68, 2017.

[17] M. S. Kim, W. J. Oh, G. Y. Baek et al., "Ultrasonic nanocrystal surface modification of high-speed tool steel (AISI M4) layered via direct energy deposition," *Journal of Materials Processing Technology*, vol. 277, Article ID 116420, 2020.

[18] P. Jovičević-Klug and B. Podgornik, "Comparative study of conventional and deep cryogenic treatment of AISI M3: 2 (EN 1.3395) high-speed steel," *Journal of Materials Research and Technology*, vol. 9, no. 6, pp. 13118–13127, 2020.

[19] H. Peng, L. Hu, T. Ngai et al., "Effects of austenitizing temperature on microstructure and mechanical property of a 4-GPa-grade PM high-speed steel," *Materials Science and Engineering A*, vol. 719, pp. 21–26, 2018.

[20] A. Michalcová, V. Pečinka, Z. Kačenka et al., "Microstructure, mechanical properties, and thermal stability of carbon-free high speed tool steel strengthened by intermetallics compared to vanadis 60 steel strengthened by carbides," *Metals*, vol. 11, no. 12, p. 1901, 2021.

[21] P. Jovičević-Klug, G. Puš, M. Jovičević-Klug, B. Žužek, and B. Podgornik, "Influence of heat treatment parameters on effectiveness of deep cryogenic treatment on properties of high-speed steels," *Materials Science and Engineering A*, vol. 829, Article ID 142157, 2022.

[22] Q. X. Dai, A. D. Wang, X. N. Cheng, and L. Cheng, "Effect of alloying elements and temperature on strength of cryogenic austenitic steels," *Materials Science and Engineering A*, vol. 311, no. 1-2, pp. 205–210, 2001.

[23] H. Halfa, "Thermodynamic calculation for silicon ModifiedAISI M2 high speed tool steel," *Journal of Minerals and Materials Characterization and Engineering*, vol. 1, no. 5, pp. 257–270, 2013.

[24] B. Sundman, B. Jansson, and J. O. Andersson, "The Thermo-Calc databank system," *Calphad*, vol. 9, no. 2, pp. 153–190, 1985.

[25] B. Sundman and J. Ågren, "A regular solution model for phases with several components and sublattices, suitable for computer applications," *Journal of Physics and Chemistry of Solids*, vol. 42, no. 4, pp. 297–301, 1981.

[26] G. C. Coelho, J. A. Golczewski, and H. F. Fischmeister, "Thermodynamic calculations for Nb-containing high-speed steels and white-cast-iron alloys," *Metallurgical and Materials Transactions A*, vol. 34, no. 9, pp. 1749–1758, 2003.

[27] J. R. Davis, Ed., *ASM Specialty Handbook: Tool Materials*, ASM international, Novelty, OH, USA, 1995.

[28] G. F. Vander Voort, S. R. Lampman, B. R. Sanders et al., "ASM handbook," *Metallography and microstructures*, vol. 9, pp. 44073–50002, 2004.

[29] S. Karagöz, H. F. Fischmeister, H. O. Andrén, and C. Guang-Jun, "Microstructural changes during over-tempering of high-speed steels," *Metallurgical Transactions A*, vol. 23, no. 6, pp. 1631–1640, 1992.

[30] C. S. Wright and R. S. Irani, "Towards equilibrium during tempering a high-speed steel," *Journal of Materials Science*, vol. 19, no. 10, pp. 3389–3398, 1984.

[31] S. Kheirandish, "Effect of Ti and Nb on the formation of carbides and the mechanical properties in as-cast AISI-M7 high-speed steel," *The Iron and Steel Institute of Japan International*, vol. 41, no. 12, pp. 1502–1509, 2001.

[32] T. Mattar, K. El-Fawakhry, H. Halfa, and M. Eissa, "Effect of nitrogen alloying on sulphur behaviour during ESR of AISI M41 steel," *Steel Research International*, vol. 79, no. 9, pp. 691–697, 2008.

[33] H. Halfa, T. Mattar, and M. Eissa, "Precipitation behavior of modified as cast high nitrogen super hard high-speed tool steel," *Steel Research International*, vol. 83, no. 11, pp. 1071–1078, 2012.

[34] H. Halfa, M. Eissa, K. El-Fawakhry, and T. Mattar, "Effect of nitrogen and niobium on the structure and secondary hardening of super hard high speed tool steel," *Steel Research International*, vol. 83, no. 1, pp. 32–42, 2012.

[35] H. Halfa, "Microstructure–wear resistance relationship of nitrogen-containing high-speed tool steel, AISIM41: non-equilibrium solidification," *Metallography, Microstructure, and Analysis*, vol. 11, no. 3, pp. 495–512, 2022.

[36] N. Broqvist, S. Hogmark, A. Medvedeva, and S. Gunnarsson, "On wear resistance of tool steel," *Journal of Manufacturing Processes*, vol. 14, no. 3, pp. 195–198, 2012.

[37] V. Knežević, J. Balun, G. Sauthoff, G. Inden, and A. Schneider, "Design of martensitic/ferritic heat-resistant steels for application at 650°C with supporting thermodynamic modelling," *Materials Science and Engineering A*, vol. 477, no. 1-2, pp. 334–343, 2008.

[38] L. S. Kremnev, "Alloying theory and its use for creation of heat-resistant tool steels and alloys," *Metal Science and Heat Treatment*, vol. 50, no. 11-12, pp. 526–534, 2008.

[39] D. Taştemur and S. Gündüz, "The effect of heat treatment on dynamic strain aging behaviour of AISI H10 hot work tool steel," *Materials Research*, vol. 21, no. 1, pp. 564–574, 2017.

[40] P. Bata and J. Pacyna, "The influence of pre–tempering on the mechanical properties of HS18-0-1 high speed steel," *Archives of Materials Science*, vol. 582, no. 28, pp. 581–584, 2007.